Linlin Liu, Jian Cheng, Jiang Xu, Paul Munroe and Zong-Han Xie

The effects of Al and Ti additions on the structural stability, mechanical and electronic properties of D8m-sStructured Ta_5Si_3

Metals, 2016; 6(6):127-1-127-18

Originally published at:
http://doi.org/10.3390/met6060127

metals

MDPI

Article

The Effects of Al and Ti Additions on the Structural Stability, Mechanical and Electronic Properties of $D8_m$-Structured Ta_5Si_3

Linlin Liu [1], Jian Cheng [1], Jiang Xu [1,2,*], Paul Munroe [3] and Zong-Han Xie [2,4,*]

1 Department of Material Science and Engineering, Nanjing University of Aeronautics and Astronautics, 29 Yudao Street, Nanjing 210016, China; liulin060410311@126.com (L.L.); 18855533109@126.com (J.C.)
2 School of Mechanical & Electrical Engineering, Wuhan Institute of Technology, 693 Xiongchu Avenue, Wuhan 430073, China
3 School of Materials Science and Engineering, University of New South Wales, Sydney NSW 2052, Australia; p.munroe@unsw.edu.au
4 School of Mechanical Engineering, University of Adelaide, Adelaide SA 5005, Australia
* Correspondence: xujiang73@nuaa.edu.cn (J.X.); zonghan.xie@adelaide.edu.au (Z.-H.X.); Tel.: +86-25-5211-2626 (J.X.); +61-883-133-980 (Z.-H.X.)

Academic Editor: Ana Sofia Ramos
Received: 6 January 2016; Accepted: 30 April 2016; Published: 26 May 2016

Abstract: In the present study, the influence of substitutional elements (Ti and Al) on the structural stability, mechanical properties, electronic properties and Debye temperature of Ta_5Si_3 with a $D8_m$ structure were investigated by first principle calculations. The Ta_5Si_3 alloyed with Ti and Al shows negative values of formation enthalpies, indicating that these compounds are energetically stable. Based on the values of formation enthalpies, Ti exhibits a preferential occupying the Ta^{4b} site and Al has a strong site preference for the Si^{8h} site. From the values of the bulk modulus (B), shear modulus (G) and Young's modulus (E), we determined that both Ti and Al additions decrease both the shear deformation resistance and the elastic stiffness of $D8_m$ structured Ta_5Si_3. Using the shear modulus/bulk modulus ratio (G/B), Poisson's ratio (υ) and Cauchy's pressure, the effect of Ti and Al additions on the ductility of $D8_m$-structured Ta_5Si_3 are explored. The results show that Ti and Al additions reduce the hardness, resulting in solid solution softening, but improve the ductility of $D8_m$-structured Ta_5Si_3. The electronic calculations reveal that Ti and Al additions change hybridization between Ta-Si and Si-Si atoms for the binary $D8_m$-structured Ta_5Si_3. The new Ta-Al bond is weaker than the Ta-Si covalent bonds, reducing the covalent property of bonding in $D8_m$-structured Ta_5Si_3, while the new strong Ti^{4b}-Ti^{4b} anti-bonding enhances the metallic behavior of the binary $D8_m$-structured Ta_5Si_3. The change in the nature of bonding can well explain the improved ductility of $D8_m$-structured Ta_5Si_3 doped by Ti and Al. Moreover, the Debye temperatures, Θ_D, of $D8_m$-structured Ta_5Si_3 alloying with Ti and Al are decreased as compared to the binary Ta_5Si_3.

Keywords: transition metal silicides; $D8_m$-Ta_5Si_3; first principle calculation; mechanical properties

1. Introduction

In order to meet the ever-increasing demand for high performing and durable structural components to be used in harsh environments, much attention has been focused upon transition metal silicides [1,2]. As the largest family of intermetallic compounds, transition metal silicides are of great interest to a wide variety of applications due to their unique properties, such as ultra-high melting temperatures, excellent electrical properties, superior thermal stability, high oxidation resistance, good creep tolerance, and excellent mechanical strength at elevated temperature [3–5]. Compared with other transition metal silicides, such as Mo and Ti silicides, that have been extensively investigated over the

past few decades, Ta-Si compounds with higher melting point than the former two silicides systems have received limited attention. As the most refractory compound in the Ta-Si binary system [6], Ta_5Si_3 has a melting point of 2550 °C, and thus has a great potential for structural applications at ultra-high temperatures. Moreover, although the high cost and density of Ta make its direct clinical application in a bulk form difficult, tantalum-based compounds are particularly suitable for use as implant coatings to improve the performance of metal substrates, due to their good corrosion resistance, exceptional biocompatibility, osseointegration properties, hemocompatibility, and high radiopacity [7]. The Ta_5Si_3 was reported to have three different polymorphs: Mn_5Si_3, W_5Si_3 and Cr_5B_3 type [8]. A $D8_8$-structured Ta_5Si_3 (Mn_5Si_3 prototype) with the $P6_3/mcm$ symmetry is a metastable phase, a $D8_1$-structured Ta_5Si_3 (Cr_5B_3 prototype) with the $I4/mcm$ symmetry is the low-temperature phase and a $D8_m$-structured Ta_5Si_3 (W_5Si_3 prototype) with the $I4/mcm$ symmetry is the high-temperature phase. Tao *et al.* [9] predicted the ductile behavior of the three prototype structures for Ta_5Si_3 and they found that the Cr_5B_3-prototype phase is slightly prone to brittleness, and the W_5Si_3-prototype phase is more prone to ductility. Therefore, in comparison to the other two prototype structures, $D8_m$-structured Ta_5Si_3 exhibits more potential as a candidate material for structural applications under an aggressive environment and has been chosen as the subject of our present work. However, as with many other intermetallic materials, owing to its strong covalent-dominated atomic bonds and intrinsic difficulties of dislocation movement, its low toughness poses a serious obstacle to its commercial application. To address this problem, several effective strategies have been developed, including densification [10,11], grain refinement [12], substitutional alloying [13], and the incorporation of a second reinforcing phase to form a composite [14]. In contrast to the ionic or covalent bonding that is prevalent in ceramics, the partial metallic character of bonding endows metal silicides with a degree of alloying ability, making it possible to improve toughness through an alloying approach. An alloying approach is achieved either by doping the metal silicides with interstitial atoms [15], or by the incorporation of substitutional atoms into the lattice of metal silicides crystal [13].

Compared with additions of interstitial atoms, incorporation of substitutional atoms into Ta_5Si_3 is more complex, and the site substitution of the added alloying elements in Ta_5Si_3 plays an important role in influencing the electronic structure and hence the mechanical properties of the material. Unfortunately, to our knowledge, no first-principles calculations have been employed to elucidate the effects of substitutional elements on the electronic structure and mechanical properties of $D8_m$-structured Ta_5Si_3. In this paper, Ti and Al were selected to investigate the site occupancy behavior of the two elements in $D8_m$-structured Ta_5Si_3 and, based upon that, the elastic moduli including bulk modulus, shear modulus, and Young's modulus were calculated for the binary and ternary Ta_5Si_3 with $D8_m$-structure. This, in turn, was used to gain insight into the effect of the two substitutional elements on the electronic structure and mechanical properties of $D8_m$-structured Ta_5Si_3.

2. Calculation Details

The first-principal calculations in this work were performed based on density functional theory (DFT) by using the Cambridge Sequential Total Energy Package code (CASTEP) [16]. The electron exchange and correlations were treated within the generalized gradient approximation using the Perdew, Burke and Ernzerhof function (GGA-PBE) [17]. The interactions between the electron and ionic cores were described by the projector augmented wave (PAW) [18] method. The ultrasoft pseudo-potentials set $5p^6 5d^3 6s^2$ for Ta, $3s^2 3p^2$ for Si, $3s^2 3p^1$ for Al and $3p^6 3d^2 4s^2$ for Ti as valence electrons, respectively, for each element. A 350 eV cutoff energy determined by the converged test for the total-energy remained constant for both the binary and ternary Ta_5Si_3 compounds. The special points sampling integration over the Brillouin zone were carried out using the Monkhorst-Pack *k*-points (the reciprocal space) mesh grid [19]. Confirming convergence to a precision of 1 meV/atom, a $4 \times 4 \times 4$ Monkhorst-Pack grid of *k*-points was adopted. Geometry optimization was processed to create a steady bulk structure with the lowest energy close to the natural structure by adjusting the lattice parameters of the models. In the optimization process, the energy change, maximum

force, maximum stress, and maximum displacement tolerances were set as 5.0×10^{-6} eV/atom, 0.01 eV/Å, 0.02 GPa and 5.0×10^{4} Å, respectively. All calculations were performed under non-spin-polarized condition.

A stoichiometric $D8_m$-structured Ta_5Si_3 unit cell consisting of 20 Ta atoms and 12 Si atoms is used for the computations. The atomic configuration of $D8_m$-structured Ta_5Si_3 is shown in Figure 1. The stacking sequence of layers along the c-axis for this structure is the same as that for $D8_m$-structured Mo_5Si_3 and can be viewed as repeated ABAC ... stacking (see Figure 1b). The A-layer has a more open atomic environment (*i.e.*, lower atomic packing density), which links together with the more close-packed B- and C-layers through the transition metal-silicon bonds [20]. Both Ta and Si have two symmetrically non-equivalent positions in the lattice. The elements that are localized on the more close-packed planes are termed Ta^{16k} and Si^{8h}, and those on the less close-packed planes are termed Ta^{4b} and Si^{4a}. For the determination of which of the doped sites is the preferential site for the alloying elements under consideration (Ti and Al). $Ta_{20}Si_{12}$ is substituted by either one Ti or one Al atom (that is, the additions concentration is 3.125 at.% (atomic concentration)), resulting in four possible substitution structures: $Ta_{19}M^{16k}Si_{12}$, $Ta_{19}M^{4b}Si_{12}$, $Ta_{20}Si_{11}M^{8h}$ and $Ta_{20}Si_{11}M^{4a}$ (M = Ti or Al). The enthalpies of formation of the four substitutional structures were calculated according to the following equation:

$$E_{form} = \frac{1}{N}(E(\mathrm{Ta}_\alpha\mathrm{Si}_\beta M) - \alpha E(\mathrm{Ta}) - \beta E(\mathrm{Si}) - E(M)) \quad (1)$$

where M denotes the alloying element Ti or Al, N represents the total atom number of $Ta_\alpha Si_\beta M$ (M is Ti or Al), and α, β means the atom number of Ta, Si. $E(Ta_\alpha Si_\beta M)$ is the value for the enthalpy of formation of $Ta_\alpha Si_\beta M$. E(Ta), E(Si) and E(M) are the ground states enthalpy of per atom for Ta, Si, Al and Ti, respectively.

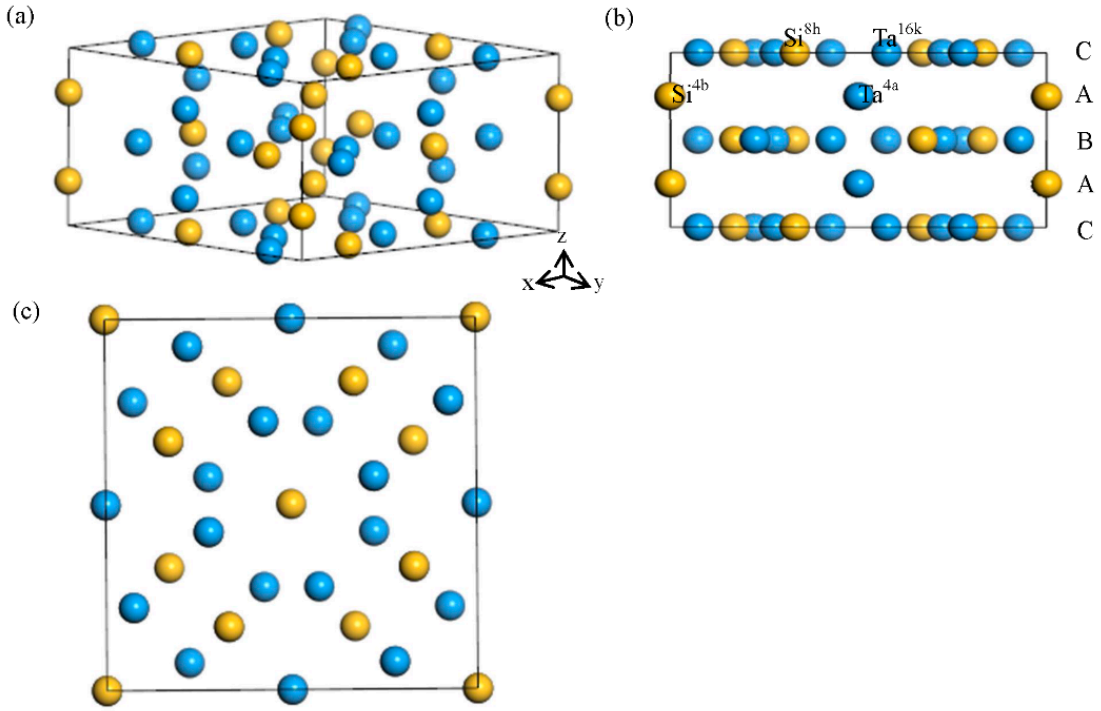

Figure 1. The crystal structure of $D8_m$ Ta_5Si_3: (**a**) 3D model; (**b**) side view; (**c**) top view. Ta atoms (**blue** balls) and Si atoms (**yellow** balls) have two symmetrically non-equivalent positions. The elements on the close-packed planes (represented by the B-layer and C-layer) are termed Ta^{16k} and Si^{8h}, and those on the less close-packed planes (represented by the A-layer) are termed Ta^{4a} and Si^{4b}.

The elastic constants can gauge the mechanical stress required to produce a given deformation. Both stress [$\sigma_{\alpha\beta}$] and strain [$\varepsilon_{\alpha\beta}$] are symmetric tensors of rank two, which can be described by matrix σ_i (i = 1, 2, . . . , 6) and ε_j (j = 1, 2, . . . , 6). As a result, the elastic constants can be represented by a 6 × 6 symmetric matrix [C_{ij}] under the conditions of small stresses and small strains:

$$\sigma_i = \sum_j C_{ij}\varepsilon_j \tag{2}$$

Meanwhile, under the conditions of small stresses and small strains on a crystal, Hooke's law is applicable and the elastic energy ΔE is a quadratic function of the strains:

$$\Delta E = V \sum_{i,j=1}^{6} \frac{1}{2} C_{ij} e_i e_j \tag{3}$$

where V is the total volume of the unit cell, e_i are the components of the strain matrix [21]

$$\varepsilon' = \begin{pmatrix} e_1 & e_6 & e_5 \\ e_6 & e_2 & e_4 \\ e_5 & e_4 & e_3 \end{pmatrix} \tag{4}$$

For the symmetry of a tetragonal crystal (a = b ≠ c, α = β = γ = 90°), there are six independent elastic constants: C_{11}, C_{12}, C_{33}, C_{13}, C_{44}, and C_{66}. In order to determine these independent elastic constants, a set of six independent total-energy calculations are performed [22]. The lattice is deformed uniformly in six different ways, and for each of them we calculated the total energy as a function of strain (up to 2%–3%). The new lattice axes a'_i are related to the original ones a'_j by $a'_i = (I + \varepsilon') \times a_j$, where I is the identity matrix and

$$\varepsilon' = \begin{pmatrix} e_1 & e_6/2 & e_5/2 \\ e_6/2 & e_2 & e_4/2 \\ e_5/2 & e_4/2 & e_3 \end{pmatrix} \tag{5}$$

Thus, if the elastic energy of a crystal is known, the elastic constants at equilibrium volumes can be calculated using Equations (2) and (3).

For the cubic symmetry (a = b = c, α = β = γ = 90°), its geometry renders some elastic constant components equal, resulting in the remaining three independent elastic constants; namely, C_{11}, C_{12} and C_{44}. The details of the calculations can be found elsewhere [9] and are not detailed here.

The effective elastic moduli of polycrystalline aggregates are usually calculated by two approximations according to Voigt [23] and Reuss [24], where uniform strain and stress are assumed throughout the polycrystal. Hill [25] has shown that the Voigt and Reuss averages are limited and suggested that the actual effective modulus can be approximated by the arithmetic mean of the two bounds, referred to as the Voigt-Reuss-Hill (VRH) value.

The Voigt bounds for the cubic system are:

$$B_V = 1/3(C_{11} + 2C_{12}) \tag{6}$$

$$G_V = 1/5(C_{11} - C_{12} + 3C_{44}) \tag{7}$$

and the Reuss bounds are:

$$B_R = 1/3(C_{11} + 2C_{12}) \tag{8}$$

$$G_R = \frac{5(C_{11} - C_{12})C_{44}}{4C_{44} + 3(C_{11} - C_{12})} \tag{9}$$

The Voigt bounds for tetragonal systems are:

$$B_V = 1/9[2(C_{11} + 2C_{12}) + C_{33} + 4C_{14})] \quad (10)$$

$$G_V = 1/30(M + 3C_{11} - C_{12} + 12C_{44} + 6C_{66}) \quad (11)$$

and the Reuss bounds are:

$$B_R = C^2/M \quad (12)$$

$$G_R = 15\{(18B_V/C^2) + [6/(C_{11} - C_{12}) + (6/C_{44}) + (3/C_{66})]\}^{-1} \quad (13)$$

$$M = C_{11} + C_{12} + 2C_{33} - 4C_{13} \quad (14)$$

$$C^2 = (C_{11} + C_{12})C_{13} - 2C_{13}^2 \quad (15)$$

For both cubic and tetragonal crystals, the VRH mean values are finally computed by:

$$B = 1/2(B_V + B_R) \quad (16)$$

$$G = 1/2(G_V + G_R) \quad (17)$$

The Young's modulus and the Poisson's ratio can be calculated based on the values of both bulk and shear modulus by the relations:

$$E = 9BG/(3B + G) \quad (18)$$

$$\upsilon = (3B - 2G)/2(3B + G) \quad (19)$$

3. Results and Discussion

3.1. Lattice Parameter

The structures of both pure elements and compounds are optimized by relaxing the simulation cell and the corresponding calculated lattice constants are obtained at a minimum energy. The phases of b.c.c tantalum, diamond-structured silicon, h.c.p titanium and f.c.c Al are used as the reference ground states. The calculated lattice constants, together with available experimental data and theoretical values, are listed in Table 1. The lattice constants of the pure elements are in good agreement with the values reported in the literature [26–30], giving confidence to the reliability of the data for this investigation. Figure 2 shows the change of unit cell volume *versus* the substitution sites occupied by one Ti or one Al atom. As shown in Figure 2, it can be seen that the change of unit cell volume is only over a range from −0.75% to 1.75%, indicating that the lattice distortion is very small when one of the four possible substitution sites is replaced by either Ti or Al. The substitution of Ti for Si in $D8_m$-structured Ta_5Si_3 slightly increases unit cell volume because the Ti atom has a larger atomic radius than the Si. After the substitution of Ti for Ta, the unit cell volume of $D8_m$-structured Ta_5Si_3 hardly changes due to a small difference of the atomic radius between Ti and Ta. The lattice expansion for Ti atom occupying the Ta^{4b} site is significantly smaller than that for Ti atom occupying the other three sites (*i.e.*, Ta^{16k}, Si^{4a} and Si^{8h}), implying a lower lattice distortion. Meanwhile, from Table 1, it is clear that only the Ti substitution for Ta^{4b} site, the lattice constants a and b are of equal value, which can maintain the tetragonal structure of $D8_m$ Ta_5Si_3. For Al substitutional alloying, it can be observed that Al substitution for Ta and Si cause lattice contraction and lattice expansion, respectively. As can be seen from Figure 2, Al atom occupying the Ta^{16k} site yields the lowest lattice distortion. However, from Table 1, only Al substitution for Si^{8h} site can retain the tetragonal structure of $D8_m$ Ta_5Si_3.

Table 1. Calculated lattice constants and enthalpies of formation for $D8_m$-structured $Ta_{20}Si_{12}$ and alloyed $D8_m$ $Ta_{20}Si_{12}$.

Phase	Type	Substitution Sites	Lattice Parameters			Enthalpy of Formation (eV/Atom)
			a (Å)	b (Å)	c (Å)	
Ta	W(A2)	-	3.309 3.306 [a]	-	-	-
Ti	-	-	2.981 2.954 [b]	-	-	-
$D8_m$ $Ta_{20}Si_{12}$	W_5Si_3	-	10.08 10.01 [c] 9.862 [d]	-	5.183 5.106 [c] 5.05 [d]	−0.619 −0.544 [c]
$Ta_{19}TiSi_{12}$	-	Ta^{16k}	10.09	10.09	5.199	−0.634
-	W_5Si_3	Ta^{4b}	10.084	-	5.197	−0.639
$Ta_{20}Si_{11}Ti$	-	Si^{4a}	10.12	10.12	5.221	−0.554
-	-	Si^{8h}	10.15	10.11	5.210	−0.557
$Ta_{19}AlSi_{12}$	-	Ta^{16k}	10.10	10.06	5.175	−0.591
-	-	Ta^{4b}	10.09	10.10	5.137	−0.602
$Ta_{20}Si_{11}Al$	-	Si^{4a}	10.08	10.15	5.199	−0.605
-	W_5Si_3	Si^{8h}	10.12	-	5.180	−0.605
Si	Si(A4)	-	5.462 5.433 [e]	-	-	-
Al	-	-	4.071 4.052 [f]	-	-	-

[a] Experiment [26]; [b] Experiment [27]; [c] Calculation [9]; [d] Experiment [28]; [e] Experiment [29]; [f] Experiment [30].

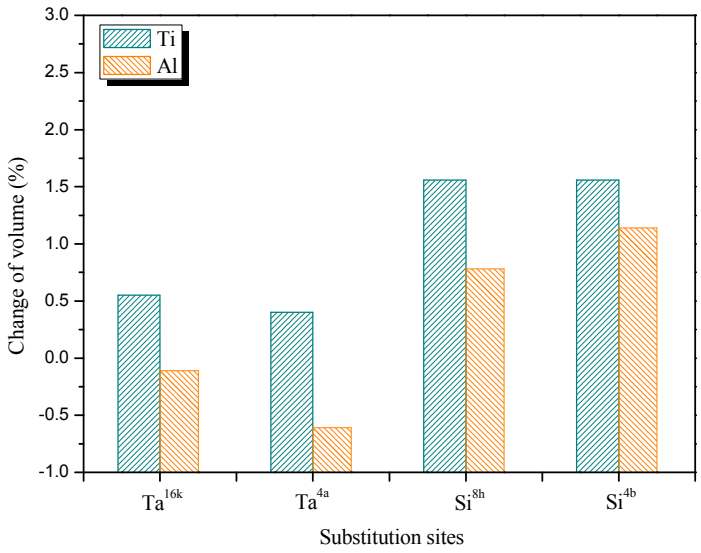

Figure 2. The change of unit cell volume for Ti and Al additions occupying the four possible substitution sites for $D8_m$-structured $Ta_{20}Si_{12}$.

3.2. Site Occupancy of Ternary Elements

It is generally assumed that the preference sites of the solute atoms are decided by their atomic radius and electronegativity. In this regard, Ti shows a preference for occupying the Ta sublattice and Al prefers to occupy the Si sublattice to maintain the minimum energy state. To confirm this assumption, the energetics of the preferential sites of M(Ti or Al) in the $D8_m$ $Ta_{20}Si_{12}$ structure can be studied based on the substitutional sites energy difference, which is defined as the difference between two different formation enthalpies [31]:

$$E_{\text{site}} = E_{\text{site-Ta}} - E_{\text{site-Si}} \quad (20)$$

where $E_{site-Ta}$ represents the formation enthalpies of $Ta_{19}MSi_{12}$ including $Ta_{19}M^{16k}Si_{12}$ and $Ta_{19}M^{4b}Si_{12}$; $E_{site-Si}$ denotes the formation enthalpies of $Ta_{20}Si_{11}M$ including $Ta_{19}Si_{11}M^{4a}$ and $Ta_{19}Si_{11}M^{8h}$ structures. If $E_{site} < 0$, occupying the Ta sublattice is energetically more favorable, and if $E_{site} > 0$, M is prone to occupying the Si sites.

Table 1 shows the enthalpy of formation for $D8_m$ $Ta_{20}Si_{12}$ which shows good agreement between experimental data [28] and theoretical results [9]. The calculations show that all of the binary and ternary $D8_m$ $Ta_{20}Si_{12}$ compounds have negative values of enthalpy of formation, meaning that all these compounds are energetically stable. Furthermore, it is clear that the E_{site} is less than zero for the Ti substitution and the enthalpy of formation of $Ta_{19}Ti^{4b}Si_{12}$ is smaller than that for $Ta_{19}Ti^{16k}Si_{12}$, implying that Ti exhibits the tendency to occupy Ta^{4b} site. In the case of one Al atom substitution, the E_{site} is larger than zero and $Ta_{20}Si_{11}Al^{8h}$ has a relatively low enthalpy of formation, suggesting that Al has a strong site preference for the Si^{8h} site.

3.3. Elastic and Mechanical Properties

The elastic properties of a solid are essential for understanding the macroscopic mechanical properties of the solid and for its potential technological applications. In order to shed some light on the influence of these two alloying elements on the mechanical properties of $D8_m$-structured Ta_5Si_3, when only one atom in $D8_m$-structured Ta_5Si_3 is substituted by ternary elements, the elastic constants of the pure elements and binary and ternary $D8_m$ Ta_5Si_3 have been calculated and are listed in Table 2. The calculated results for b.c.c Ta and diamond-structured Si are in good consistence with the experimental data [32,33] and the elastic properties for the alloying element Al are comparable to the values reported by Kang *et al.* [34], which is indicative of the reliability and accuracy of the theoretically predicted results. As is well known, the elastic stability is a necessary condition for a stable crystal. For the tetragonal system, the mechanical stability criteria are decided by the following restrictions of its elastic constants, $C_{11} > 0$, $C_{33} > 0$, $C_{44} > 0$, $C_{66} > 0$, $C_{11} - C_{12} > 0$, $(C_{11} + C_{33} - 2C_{13}) > 0$, and $2(C_{11} + C_{12}) + C_{33} + 4C_{13} > 0$. The calculated elastic constants of all the binary and ternary $D8_m$-structured Ta_5Si_3 compounds satisfy the above criteria, indicating that these compounds are mechanically stable. The elastic constants provide valuable information about the bonding character between adjacent atomic planes and the anisotropic character of the bonding. It can be seen from Table 2 that the values of C_{11} are larger than that of C_{33}, which indicates that their *a*-axis direction ([100] direction) and *b*-axis direction ([010] direction) are stiffer than *c*-axis direction ([001] direction). The values of $(C_{11} + C_{12})$ are greater than that of C_{33}, suggesting that the elastic modulus is higher in the (001) plane than along [001] direction. Regardless of the binary and ternary $D8_m$-structured Ta_5Si_3 compounds, the values of C_{66} is larger than C_{44}, indicating that the [100](001) shear is easier than the [100](010) shear. The elastic anisotropy of the transition metal silicides has an important impact on the mechanical properties of the systems, especially on dislocation structures and mechanisms [35]. The anisotropy factors for tetragonal phases can be estimated as $A = 2C_{66}/(C_{11} - C_{12})$. A is equal to one for an isotropic crystal. The values of A are 1.03, 1.09 and 1.13 for the $Ta_{20}Si_{12}$, $Ta_{20}Si_{11}Al^{8h}$ and $Ta_{19}Ti^{4b}Si_{12}$, indicating that the shear elastic properties of the (001) plane are nearly independent of the shear direction for all the binary and ternary $D8_m$-structured Ta_5Si_3 compounds. Similar properties have been found for the $D8_m$-structured phase of V_5Si_3 [36] and Mo_5Si_3 [37].

Based on the calculated elastic constants, the bulk modulus (*B*), shear modulus (*G*) and Young's modulus (*E*) for binary and ternary $D8_m$-structured Ta_5Si_3 are calculated based on the Voigt–Reuss–Hill approximation, and are shown in Figure 3. The calculated values for the bulk modulus (*B*), shear modulus (*G*) and Young's modulus (*E*) for $D8_m$-structured Ta_5Si_3 are also in good agreement with the previous calculations [9]. Therefore, with respect to the available data, the present calculations yield comparable values. The substitution of Ta by Ti simultaneously lowers the values of *B*, *G*, and *E*, while the substitution of Si by Al also lowers the values of *G* and *E*, but slightly enhances the value of B. Since bulk moduli are generally believed to be related to the cohesive energy of materials, the variation of bulk modulus is related to changes in cohesive strength between atoms [38]. The binary Ta_5Si_3

has the largest values of shear modulus and Young's modulus, confirming that it has a higher shear deformation resistance and elastic stiffness as compares to ternary Ta_5Si_3 compounds. The ductility or brittleness of a solid is very important, because ductile materials are more resistant to catastrophic failure under critical mechanical stress conditions. There is no universally accepted criterion to gauge ductility or brittleness of a given material purely based on elastic data derived from linear elastic theory, but a reasonable representation of it can be realized by ratio of bulk/shear modulus B/G proposed by Pugh [39]. According to Pugh's empirical rule, the critical number of this parameter separating the ductile and brittle nature of a material is 1.75. If $B/G > 1.75$, the material behaves in a ductile manner; otherwise, the material deforms in a brittle mode. As shown in Figure 4, the B/G ratios for all of binary and ternary Ta_5Si_3 compounds are slightly larger than this critical value, implying that all of binary and ternary Ta_5Si_3 compounds exhibit ductile behavior. Meanwhile, the additions of Ti and Al further increase in the calculated B/G ratios, suggesting that both Ti and Al are beneficial to the improvement of ductility of the Ta_5Si_3 compound. Based on the values of B/G, the addition of Al is more efficient than Ti addition to improve the ductility of Ta_5Si_3. Poisson's ratio (υ) is associated with the volume change during uniaxial deformation and has been used to quantify the stability of the crystal against shear. In addition, Poisson's ratio provides more information about the degree of directionality of the covalent bonding than any of the other elastic coefficients and its value can also be employed to evaluate the ductility or brittleness of materials [40]. It is generally assumed that when υ is less than 0.26, the material is brittle, and at higher values it is ductile. The variation of the values of Poisson's ratios for the binary and ternary Ta_5Si_3 compounds is the same as those for B/G ratios. The results indicate that the additions of Ti and Al reduce the directionality of atomic bonding of Ta_5Si_3 and the directionality in atomic bonding in Ta_5Si_3 alloyed with Al is weaker than that in Ta_5Si_3 alloyed with Ti. Cauchy pressure ($C_{12} - C_{44}$) describes the angular characteristics of interatomic bonds in metals and compounds, thus serving as an indication of ductility. According to Pettifor [41], if the value of Cauchy pressure is positive, the material is expected to be ductile in nature; otherwise, it is brittle in nature. It can be seen from Figure 5 that the values of Cauchy pressure for the binary and ternary Ta_5Si_3 compounds is positive, further confirming that they are expected to be ductile in nature.

Table 2. Calculated elastic constants for the binary, ternary $D8_m$-structured $Ta_{20}Si_{12}$ and their constituent elements compared to the data obtained experimentally and theoretically.

Structural	Ta (BCC)	Si (Diamond)	Al (FCC)	Ti (Hexagonal)	$Ta_{20}Si_{12}$	$Ta_{19}Ti^{4b}Si_{12}$	$Ta_{20}Si_{11}Al^{8h}$
C_{11} (GPa)	260 266 [a]	160 168 [b]	102 97 [c]	196	386.80 410.19 [d]	365.51	378.39
C_{12} (GPa)	149 158 [a]	70 65 [b]	70 62 [c]	57	137.12 145.66 [d]	133.36	137.31
C_{13} (GPa)	-	-	-	69.59	106.55 125.45 [d]	112.33	116.75
C_{33} (GPa)	-	-	-	200.12	339.40 338.89 [d]	298.14	317.29
C_{44} (GPa)	85 87 [a]	75 80 [b]	22 21 [c]	45.98	86.68 92.94 [d]	84.55	85.22
C_{66} (GPa)	-	-	-	69.86	128.03 132.91 [d]	130.85	131.50

[a] Experiment [32]; [b] Experiment [33]; [c] Calculation [34]; [d] Calculation [9].

As one of the most basic mechanical properties of a material, hardness of a given material is characterized by the ability to resist to both elastic and irreversible plastic deformations, when a force is applied [42]. Some researchers have tried to create a correlation between hardness and elasticity [43,44]. For the partially covalent transition metal-based materials, since the shear modulus scales with the stresses required to nucleate or move isolated dislocations and hence is proportional to the hardness, it is regarded as a good indicator of hardness [45]. Thus, in the term of the values of shear modulus, the hardness increases in the following sequence: $Ta_{20}Si_{11}Al^{8h} < Ta_{19}Ti^{4b}Si_{12} < Ta_{20}Si_{12}$. Chen *et al.* [46] assumed that unlike the moduli of G and B, which only measured the elastic response, the Pugh's modulus ratio (B/G) seemed to correlate much more reliably with hardness because it responded to

both elasticity and plasticity, which were the most intrinsic features of hardness. They proposed a semiempirical formula to calculate Vickers hardness of polycrystalline materials:

$$H_v = 2(k^{-2}G)^{0.585} - 3 \quad (21)$$

where k denotes the Pugh's modulus ratio, B/G. The Vickers hardness values calculated from Equation (21) are presented in Figure 5. The values of Vickers hardness for $Ta_{20}Si_{11}Al^{8h}$, $Ta_{19}Ti^{4b}Si_{12}$ and $Ta_{20}Si_{12}$ are estimated to 11.40, 11.48 and 12.27 GPa. Again, the calculated results predict that Ti and Al substitutions result in solid solution softening.

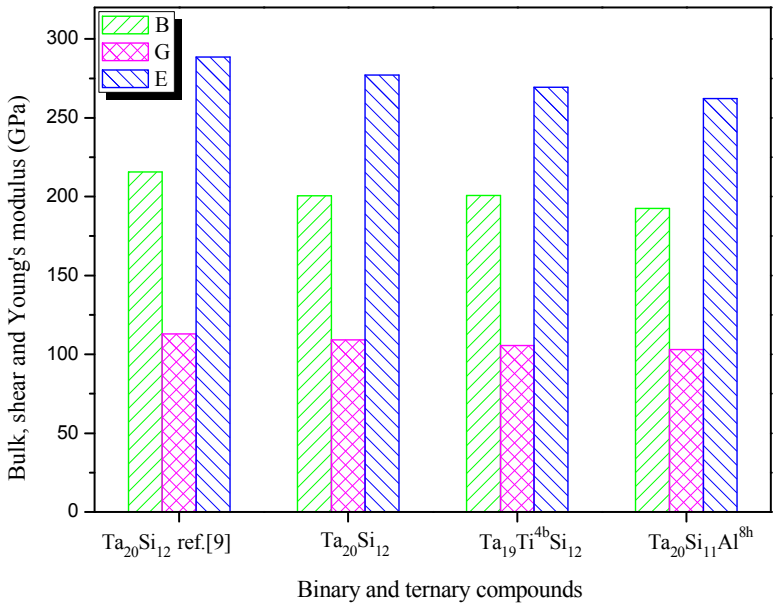

Figure 3. Calculated bulk modulus (B), shear modulus (G) and Young's modulus (E) for the binary and ternary $D8_m$-structured $Ta_{20}Si_{12}$.

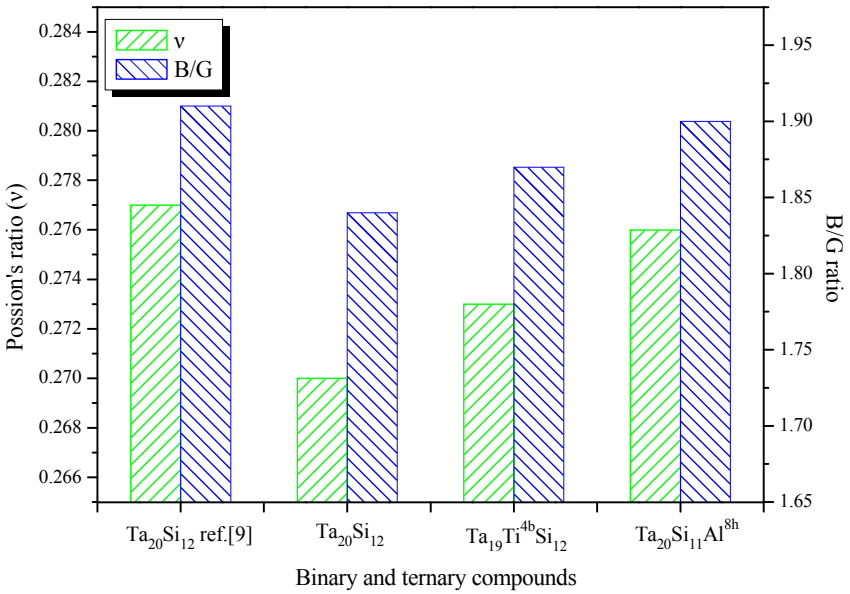

Figure 4. The Poisson's ratio, ν, and the Pugh modulus ratio, B/G, for $Ta_{20}Si_{12}$, $Ta_{20}Si_{11}Al^{8h}$ and $Ta_{19}Si_{12}Ti^{4b}$. Theoretical values reported in the literature [8] are shown in the figure for comparison.

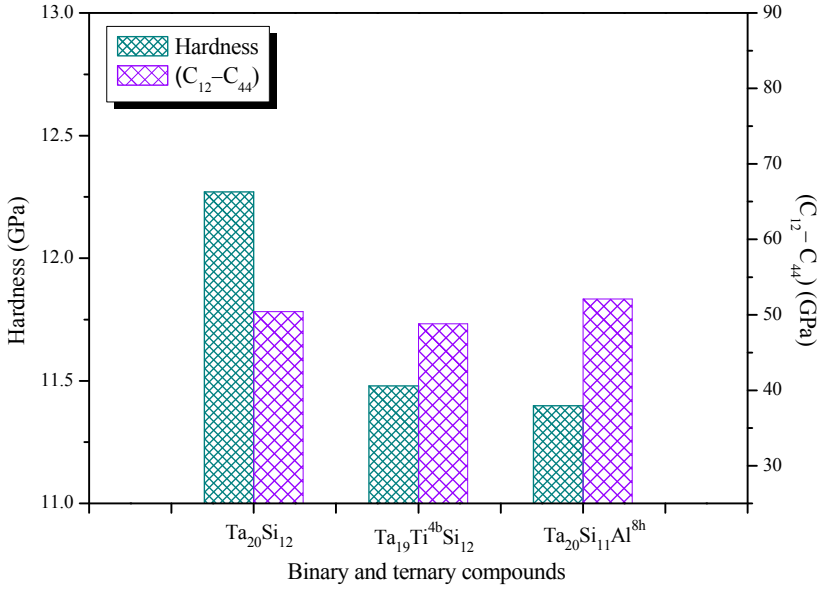

Figure 5. The Vickers hardness and Cauchy's pressure ($C_{12} - C_{44}$) for $Ta_{20}Si_{12}$, $Ta_{19}Ti^{4b}Si_{12}$ and $Ta_{20}Si_{11}Al^{8h}$.

3.4. Electronic Structure and Population Analysis

Mechanical properties of a material reflect its resistance to elastic and plastic deformation, which are controlled, in part, by the chemical bonding that is, in turn, determined by electronic structures. Hence, in order to gain insight into the mechanisms governing the mechanical properties of the binary and ternary $D8_m$-structured Ta_5Si_3, the electronic structures of these materials were investigated and compared. Figures 6 and 7 present the calculated total and partial density of states (DOS) for the binary and ternary $D8_m$-structured Ta_5Si_3, where the black vertical dashed of DOS represents the Fermi level. The pseudogap (the low valley near the Fermi level) is likely to split the bonding and anti-bonding states. As shown in Figure 6, the introduction of either an Al atom or a Ti atom pushes the Fermi level towards a lower energy side of the pseudogap, denoting that some bonding states may be occupied by electrons from anti-bonding states. Compared with the binary Ta_5Si_3, the total DOS for ternary Ta_5Si_3 have two new peaks of bonding states near −6 and −2 eV and a new peak of bonding states near −2 eV, respectively. As can be seen from Figure 7a, the partial densities of states (PDOS) profile of binary Ta_5Si_3 mainly divides into three parts. The first part is from −12 to −6.7 eV, consisting mainly of Ta-5*d* states, Si-3*s* states, and part of Si-3*p* states. For the second part, the main bonding states located between −6.7 and −1.0 eV are dominated by Ta-*5d* states, Si-*3p* states and part of Ta-5*p*. The third part ranging from −1.0 to 2 eV is contributed mainly by Ta-5*d* states and part of Si-*3p* states. For the first part, the hybridization focuses on Ta-5*d* states and Si-3*s* states, forming Ta-Si bond. It is to be noted here that Si-3*s* states plays an important role in charge transfer. The second and third parts are different from the first part. In the second and third parts, the charge of Si atom transfers from 3*s* to 3*p* states and the Ta-5*d* states play an important role in electronic contribution. The hybridization between Ta-5*d* states and Si-3*p* states forms Ta-Si bond. In the last part, the anti-bonding states dominated by Ta-5*d* states forms Ta-Ta anti-bonding. For the PDOS profile of $Ta_{20}Si_{11}Al^{8h}$ (Figure 7b), the bonding states from −6 to −7 eV originate mainly from Ta-5*s* states and Al-3*s* sates, indicating strong electronic interactions for Ta-Al bonding. The Ta5*s*-Al3*s* bonding contribute to the new peak of bonding states near −6 eV in total DOS of $Ta_{20}Si_{11}Al^{8h}$ compound (Figure 7b). States from −6.2 to 2eV are dominated by Ta-*5d*, Si-*3p* and Al-3*p* states. Furthermore, the hybridized Al-3*p* and Ta-5*d* states occur in an energy range that is higher than that of the hybridized Si-3p and Ta-5d states, suggesting that the Al3*p*-Ta5*d* bonds are weaker than that of the Si3*p*-Ta5*d* bonds, reducing the covalent property of bonding in $D8_m$-structured Ta_5Si_3. The formation of the weaker Al-Ta covalent bonds explains why the ductility of the Ta_5Si_3 alloyed

with Al is better than that of binary Ta_5Si_3. In the partial DOS profile of $Ta_{19}Ti^{4b}Si_{12}$ (Figure 7c), the Ti-3*d* states near −2 eV hybridize with Si-3*p* states, contributing to formation of the peak of bonding states in the total DOS of $Ta_{19}Ti^{4b}$ Si_{12}(Figure 7b). The anti-bonding states are dominated by Ti-3*d* and Ta-5*d* states, showing evidence for the formation of strong Ti-Ta anti-bonding. Moreover, these Ti-Ta anti-bonding states occupy some bonding states between Ta and Si in the total DOS profile of $Ta_{19}Ti^{4b}Si_{12}$ as compares to binary $D8_m$ $Ta_{20}Si_{12}$, weakening the covalent property of bonding in $D8_m$ $Ta_{20}Si_{12}$. The strong Ti-Ta anti-bonding and the reduction of covalent property should be responsible for the improvement of ductility.

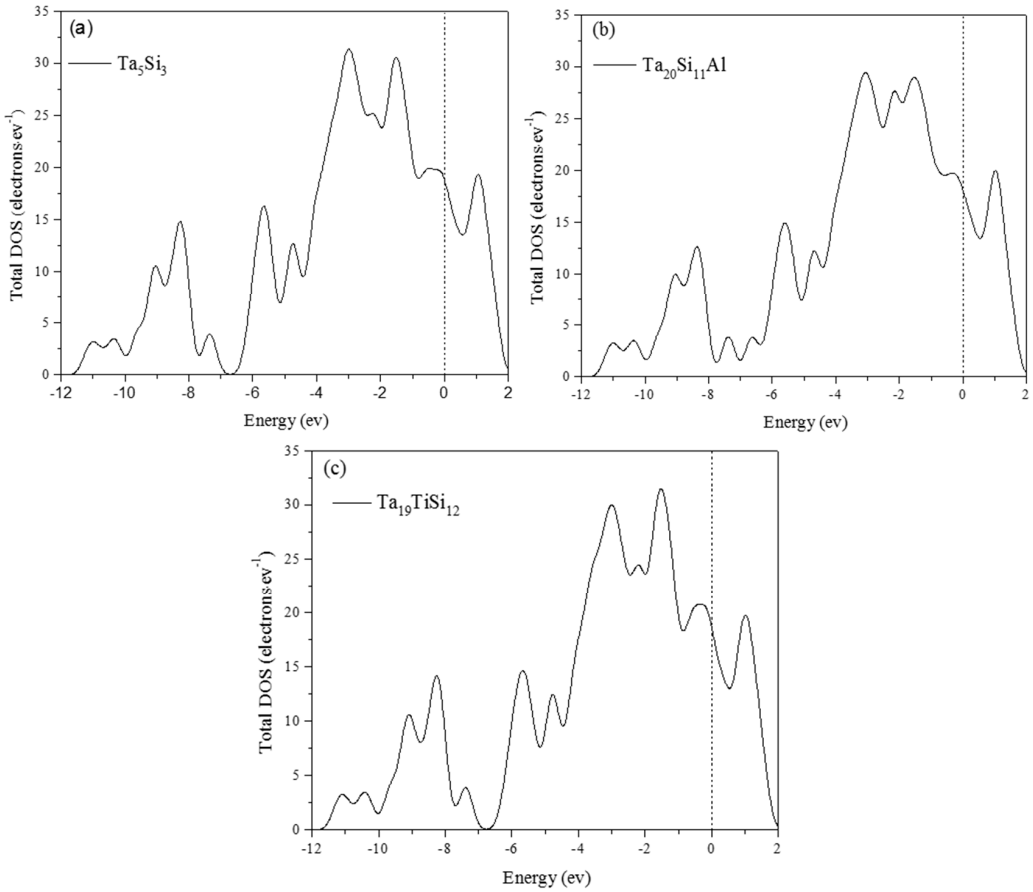

Figure 6. Calculated total density of states (DOS) for (**a**) $Ta_{20}Si_{12}$; (**b**) $Ta_{20}Si_{11}Al^{8h}$ and (**c**) $Ta_{19}Si_{12}Ti^{4b}$.

To further reveal the charge transfer and the chemical bonding properties of both non-doped and doped Ta_5Si_3, the difference in bonding charge density for the three compounds was investigated. The bonding charge density, also called the deformation charge density, is defined as the difference between the self-consistent charge density of the interacting atoms in the crystal and a reference charge density constructed from the superposition of the non-interacting atomic charge density at the lattice sites [47]. The distribution of the bonding charge densities in the (001) plane along the a- and b-axis for non-doped and doped Ta_5Si_3 is given in Figures 8 and 9 where the red region denotes a high charge density and the blue region denotes a relatively low charge density. It is noted in Figure 8 that the bonding charge density shows a depletion of the electronic density at the lattice sites together with an increase of the electronic density in the interstitial region. It is also noted that the bonding charge build-up in the Ta^{16k}-Si^{8h}-Ta^{16k} planar triangular bonding area is strong. This feature is consistent with the PDOS plots in Figure 7a, showing the importance of the hybridization between Ta^{16k}-5*d* states and Si^{8h}-3*p* states, forming the Ta^{16k}-Si^{8h} bonds.

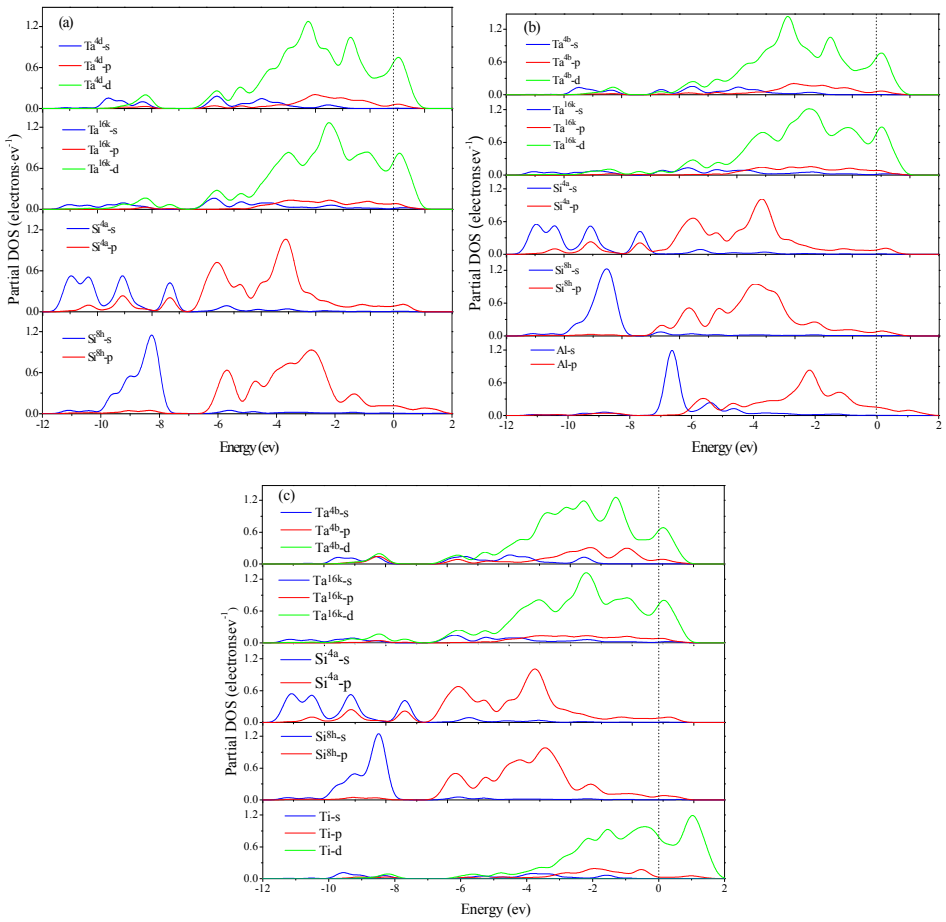

Figure 7. Calculated partial density of states (DOS) for (**a**) $Ta_{20}Si_{12}$; (**b**) $Ta_{20}Si_{11}Al^{8h}$ and (**c**) $Ta_{19}Ti^{4b}Si_{12}$.

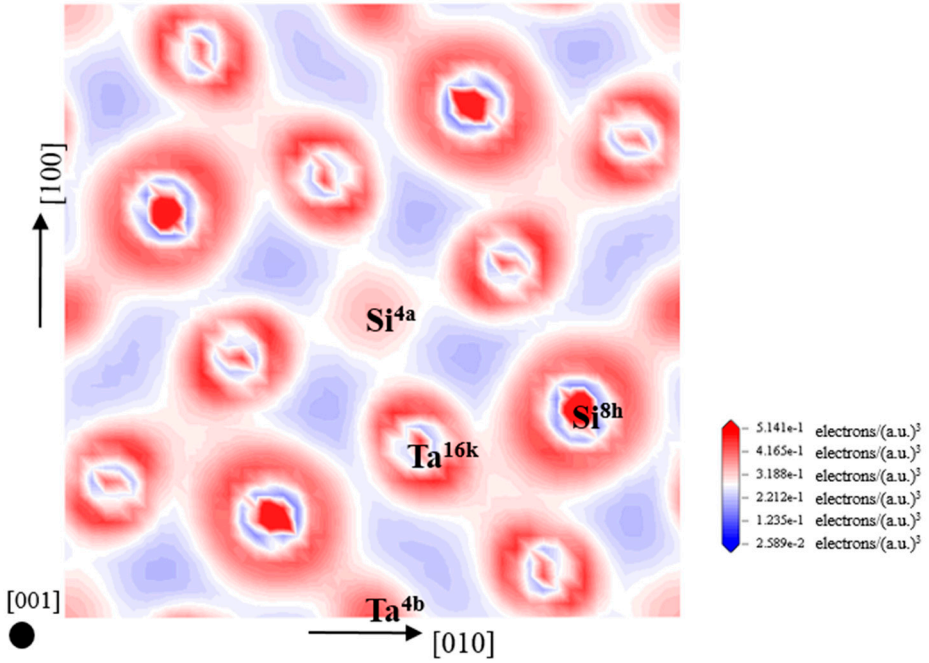

Figure 8. The difference density of contour plots for $Ta_{20}Si_{12}$ unit cell in the (001) plane. ● denotes the direction perpendicular paper from inside to outside. The Ta^{4b}, Ta^{16k}, Si^{4a} and Si^{8h} symbols designate the positions of, respectively, Ta in the 4b site, Ta in the 16k site, Si in the 4a, and Si in the 8h site.

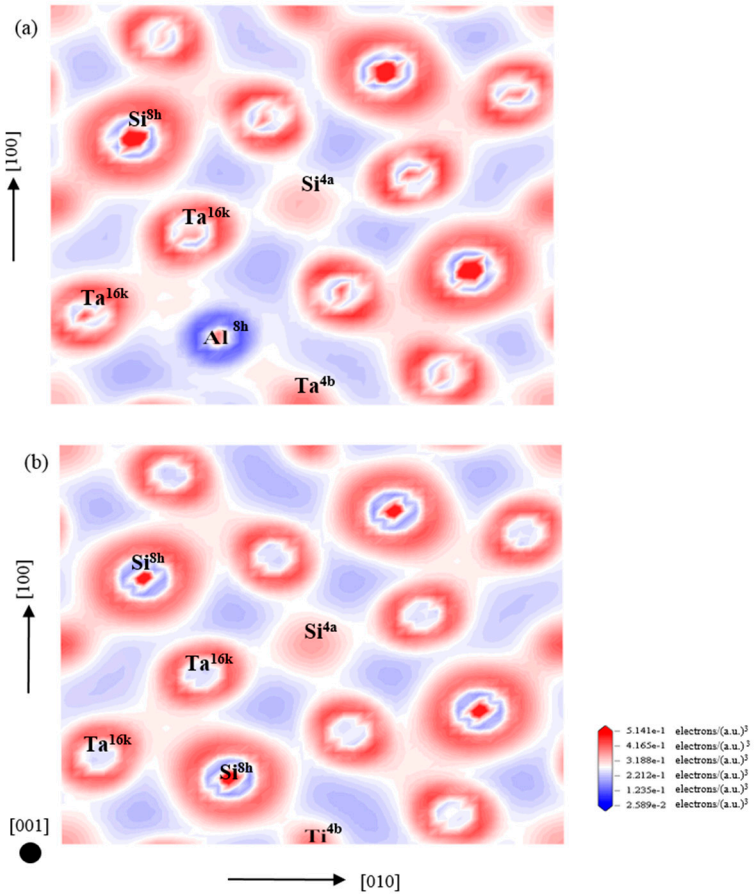

Figure 9. The difference density of contour plots for (**a**) $Ta_{20}Si_{11}Al^{8h}$ and (**b**) $Ta_{19}Ti^{4b}Si_{12}$ unit cell in (001) plane. ● denotes the direction perpendicular paper from inside to outside. The Ta^{4b}, Ta^{16k}, Si^{4a}, Si^{8h}, Al^{8h} and Ti^{4b} symbols designate the positions of, respectively, Ta in the 4b site, Ta in the 16k site, Si in the 4a, Si in the 8h site, Al in the 8h site and Ti in the 4b site.

After replacing a Si atom in the 8h site with an Al atom, a significant redistribution of the bonding charge in the interstitial region is seen in Figure 9a. The region around the substitution lattice site changes from red to blue, meaning that the charge density around the Al atom is much sparser than that around the Si atom. In addition, Ta^{16k}-Al^{8h}-Ta^{16k} planar triangular bonding area is weaker than the Ta^{16k}-Si^{8h}-Ta^{16k} planar triangular bonding area. This result is consistent with the view derived from the DOS plots that the strength of Al-Ta bonds is weaker than that of the Si-Ta bonds. When one Ta^{4a} site is occupied by a Ti atom, see Figure 9b, the region between substitution site and Si^{8h} site is almost near-white, showing the decline of the interacting atomic charge density for the Ti^{4b}-Si^{8h} planar bonding area as compares with Ta^{4b}-Si^{8h} planar bonding area.

Mulliken [48] analyzed correlations of overlap population with the degree of covalency of bonding and bond strength. The bonding (anti-bonding) states related to positive (negative) values of bond population, and the low (high) values imply that the chemical bond exhibits strong ionic (covalent) bonding [49].

As seen in Table 3, the covalent character for the binary and ternary Ta_5Si_3 are mainly attributed to the Ta^{16k}-Si^{8h} covalent bond with high overlap population and the highest bond number. The above discussion about DOS for $Ta_{19}Ti^{4b}Si_{12}$ indicates that the Ti substitution changes the anti-bonding states between the Ta atoms. This observation is confirmed by the following changes in the populations of bonds: (a) the number of metallic bonds Ta^{16k}-Ta^{16k} increases by four and its overlap population exhibits a significant decease; (b) a new strong anti-bonding Ti^{4b}-Ta^{4b} appears in the network of metallic bonds with the disappearance of weak Ta^{4b}-Ta^{4b} anti-bonding. The change (a) weakens the

covalent character of $Ta_{19}Ti^{4b}Si$ and improves its metallic properties and (b) improves the metallic property of the 4b-4b bonds. Clearly, those Ta-Ta metallic bonds including Ta^{16k}-Ta^{16k} and Ta^{4b}-Ta^{4b} anti-bonding lower the deformation resistance, thereby reducing the elastic properties. Consequently, the change seen in both (a) and (b) intensifies the metallic property of bonds for the $Ta_{19}Ti^{4b}Si_{12}$ compound, resulting in a decrease of the elastic properties and an increase in ductility for $Ta_{19}Ti^{4b}Si_{12}$. In addition, the hybridization between Ti-3*d* and Si-3*p* forms four new Ti^{4b}-Si^{8h} bonds of which the overlap population are close to zero. This also means a decrease in covelency for $Ta_{19}Ti^{4b}Si_{12}$ compared with $Ta_{20}Si_{12}$. In the case of Si site substitution, the bonding length and the overlap populations of Si^{8h}-Ta^{16k} bonds becomes longer and smaller and the bonding length of the Ta^{16k}-Ta^{16k} metallic bonds becomes shorter, indicating that the Si^{8h}-Ta^{16k} bonds get weaker leading to charge transfer towards the Ta^{16k}-Ta^{16k} bonds. As such, the covalent character of 8h-16k bonds becomes weaker and Ta^{16k}-Ta^{16k} bonds become stronger, resulting in the improvement of ductility for $Ta_{20}Si_{11}Al^{8h}$.

Table 3. Mulliken overlap populations, bond lengths and numbers of bonds calculated for $Ta_{20}Si_{12}$, $Ta_{20}Si_{11}Al^{8h}$ and $Ta_{19}Ti^{4b}Si_{12}$ compounds.

Bond	$Ta_{20}Si_{12}$			$Ta_{20}Si_{11}Al^{8h}$			$Ta_{19}Ti^{4b}Si_{12}$		
	P	L	N	P	L	N	P	L	N
Ta^{4b}-Ta^{4b}	−0.08	2.592	2	0.01	2.597	2	0.01	2.599	1
Ta^{16k}-Ta^{16k}	0.46	2.918	8	0.45	2.903	8	0.34	2.965	12
Si^{4a}-Si^{4a}	0.41	2.592	2	0.40	2.598	2	0.40	2.599	2
Si^{4a}-Ta^{16k}	0.19	2.677	32	0.19	2.677	32	0.19	2.682	32
Ta^{4b}-Si^{8h}	0.31	2.677	16	0.31	2.69	14	0.35	2.696	12
Si^{8h}-Ta^{16k}	0.35	2.833	48	0.33	2.832	43	0.40	2.78	43
Al^{8h}-Ta^{4b}		-		0.30	2.735	2		-	
Al^{8h}-Ta^{16k}		-		0.41	2.930	6		-	
Ti^{4b}-Si^{8h}		-			-		0.13	2.678	4
Ti^{4b}-Ta^{4b}		-			-		−0.24	2.599	1

Data in the Table 3 are average values; P: Mulliken populations; L: Bond length (Å); N: Numbers of bonds.

3.5. Debye Temperature

As a fundamental parameter, the Debye characteristic temperature correlates with many physical properties of solids, such as specific heat, elastic constants and melting temperature [50]. Elastic and thermal properties are inseparable because they both originate in the lattice vibrational spectrum of a solid. Therefore, the Debye temperature can be determined from the elastic constants. Theoretically, the Debye temperature (Θ_D), at T = 0 K, can be calculated by using the average sound velocity (ν_m) from the following relationship:

$$\Theta_D = \frac{h}{k_B}\left[\frac{3n}{4\pi}\left(\frac{N_A\rho}{M}\right)\right]^{\frac{1}{3}} \times \upsilon_m \tag{22}$$

here, h and k_B represent the Planck and Boltzmann constants; n is the number of atoms in per formula unit, N_A is Avogadro's number, M is the mass of per formula unit. The density, ρ, can be obtained based on a knowledge of the unit cell lattice parameters. The parameter ν_m represents the average sound velocity which is defined as:

$$\upsilon_m = \left[\frac{1}{3}\left(\frac{1}{\upsilon_l^3} + \frac{2}{\upsilon_s^3}\right)\right]^{-\frac{1}{3}} \tag{23}$$

where υ_l and υ_s are the longitudinal and transverse sound velocities respectively, which can be obtained by bulk modulus (B) and shear modulus (G)

$$v_l = \left(\frac{B + \frac{4}{3}G}{\rho} \right) \text{ and } v_s = \left(\frac{G}{\rho} \right)^{\frac{1}{2}} \quad (24)$$

The calculated longitudinal, transverse and average sound velocities and Debye temperature of both non-alloyed and alloyed $D8_m$-structured Ta_5Si_3 and their constituent elements were calculated and are listed in Table 4. The results obtained agree well with previous studies [8,51,52]. The Debye temperatures of the three compounds are larger than that of tantalum. This is because the mass-density of Ta (16.58 g/cm^3) is larger than that of these compounds (around 12.5 g/cm^3), so that sound velocity in Ta is lower, that is, this leads to a lower Debye temperature. In contrast, Si and Al have relatively much lower densities (2.286 and 2.66 g/cm^3, respectively), resulting in larger Debye temperatures. Compared to the $D8_m$-structured Ta_5Si_3, the ternary Ta_5Si_3 compounds have lower Debye temperatures. Different Θ_D-values indicate different lattice dynamics or degrees of lattice stiffness [53]. Thus, the reasons for the observed decrease of Θ_D can be mainly attributed to structural softening and the relative low shear modulus (shown in Table 4), which results in a lower cut-off for the atomic vibrational frequency [54].

Table 4. Calculated density ρ (in g/cm^3), longitudinal, transverse, average sound velocities (in m/s) and Debye temperature Θ_D (in K) for the binary, ternary $D8_m$-structured $Ta_{20}Si_{12}$ and its constituent elements.

Phase	Ta	Si	Al	Ti	$Ta_{20}Si_{12}$	$Ta_{20}Si_{11}Al^{8h}$	$Ta_{19}Ti^{4b}Si_{12}$
ρ	16.58	2.286	2.66	4.56	12.5	12.5	12.1
v_l	5827	8906	6474	6398	5262	5227	5221
v_t	2940	5166	2980	3561	2954	2906	2918
v_m	3296	5733	3357	3965	3287	3236	3248
Θ	374 253 [a]	626 635 [a]	390 428 [b]	450 374 [b]	385 388 [c]	380	381

[a] Experiment [51]; [b] Calculation [52]; [c] Calculation [9].

4. Conclusions

In summary, the influence of substitutional alloying elements (Ti and Al) on the structural stability, mechanical properties, electronic properties and Debye temperature of Ta_5Si_3, exhibiting a $D8_m$ structure, were systematically investigated by first principle calculations. All of the binary and ternary Ta_5Si_3 compounds show negative enthalpy of formation values, indicating that these compounds are energetically stable. Based on the values of formation enthalpies, Ti exhibits a preferential occupying the Ta^{4b} site and Al has a strong site preference for the Si^{8h} site. The calculated results for the elastic constants show that doping with Ti simultaneously lowers the B, G, and E values of $D8_m$-structuted Ta_5Si_3. The variation of the shear modulus and the Young's modulus of this compound with an Al addition has a similar tendency to that of a Ti addition, although an Al addition slightly enhances the bulk modulus. The change of the ductility of the $D8_m$-structured Ta_5Si_3 is explained according to the shear modulus/bulk modulus ratio (G/B), the Poisson's ratio and the Cauchy's pressure. The results show that ductility was improved by doping with Ti and Al. Moreover, the hardness of the Ta_5Si_3 is reduced by both Ti and Al additions, resulting in solid solution softening. Electronic structure analysis indicates that alloying with Ti and Al introduces a more metallic nature to the bonding, resulting in the enhancement in ductility of $D8_m$ Ta_5Si_3. Moreover, the Debye temperatures, Θ_D, of $D8_m$-structured Ta_5Si_3 alloying with Ti and Al are decreased as compared to the binary Ta_5Si_3.

Acknowledgments: The authors acknowledge the financial support from the National Natural Science Foundation of China under Grant No. 51374130. This work is supported by Funding of Jiangsu Innovation Program for Graduate Education, the Fundamental Research Funds for the Central Universities (CXLX13-151). This study is also supported by the Australian Research Council Discovery Project (DP150102417).

Author Contributions: Linlin Liu, Jian Cheng and Jiang Xu conceived and designed the experiments; Linlin Liu performed the experiments; Linlin Liu and Jian Cheng analyzed the data; Paul Munroe and Zong-Han Xie contributed reagents, materials and analysis tools; Linlin Liu, Jian Cheng and Jiang Xu wrote the paper.

Conflicts of Interest: The authors declare no conflict of interest.

References

1. Nakano, T.; Azuma, M.; Umakoshi, Y. Tensile deformation and fracture behaviour in $NbSi_2$ and $MoSi_2$ single crystals. *Acta Mater.* **2002**, *14*, 3731–3742. [CrossRef]
2. Xu, J.; Leng, Y.; Li, H.; Zhang, H. Preparation and characterization of SiC/(Mo, W)Si_2 composites from powders resulting from a SHS in a chemical oven. *Int. J. Refract. Met. Hard Mater.* **2009**, *27*, 74–77. [CrossRef]
3. Datta, M.K.; Pabi, S.K.; Murty, B.S. Thermal stability of nanocrystalline Ni silicides synthesized by mechanical alloying. *Mater. Sci. Eng. A* **2000**, *1*, 219–225. [CrossRef]
4. Mason, K.N. Growth and characterization of transition metal silicides. *Prog. Cryst. Growth Charact. Mater.* **1981**, *2*, 269–307. [CrossRef]
5. Fujiwara, H.; Ueda, Y. Thermodynamic properties of molybdenum silicides by molten electrolyte EMF measurements. *J. Alloy. Compd.* **2007**, *441*, 168–173. [CrossRef]
6. Schlesinger, M.E. The Si-Ta (silicon-tantalum) system. *J. Phase Equilib.* **1994**, *15*, 90–95. [CrossRef]
7. Matsuno, H.; Yokoyama, A.; Watari, F.; Uo, M.; Kawasaki, T. Biocompatibility and osteogenesis of refractory metal implants, titanium, hafnium, niobium, tantalum and rhenium. *Biomaterials* **2001**, *22*, 1253–1262. [CrossRef]
8. Tillard, M. The mixed intermetallic silicide $Nb_{5-x}Ta_xSi_3$ ($0 \leqslant x \leqslant 5$). Crystal and electronic structure. *J. Alloy. Compd.* **2014**, *584*, 385–392. [CrossRef]
9. Tao, X.; Jund, P.; Viennois, R.; Catherine, C.; Tedenacet, J.C. Physical properties of thallium–tellurium based thermoelectric compounds using first-principles simulations. *J. Phys. Chem. A* **2011**, *31*, 8761–8766. [CrossRef] [PubMed]
10. Mitra, R. Microstructure and mechanical behavior of reaction hot-pressed titanium silicide and titanium silicide-based alloys and composites. *Metall. Mater. Trans. A* **1998**, *6*, 1629–1641. [CrossRef]
11. Rosenkranz, R.; Frommeyer, G.; Smarsly, W. Microstructures and properties of high melting point intermetallic Ti_5Si_3 and $TiSi_2$ compounds. *Mater. Sci. Eng. A* **1992**, *1*, 288–294. [CrossRef]
12. Korznikov, A.V.; Pakieła, Z.; Kurzydłowski, K.J. Influence of long-range ordering on mechanical properties of nanocrystalline Ni_3Al. *Scr. Mater.* **2001**, *45*, 309–315. [CrossRef]
13. Dasgupta, T.; Umarji, A.M. Thermal properties of $MoSi_2$ with minor aluminum substitutions. *Intermetallics* **2007**, *15*, 128–132. [CrossRef]
14. Gutmanas, E.Y.; Gotman, I. Reactive synthesis of ceramic matrix composites under pressure. *Ceram. Int.* **2000**, *7*, 699–707. [CrossRef]
15. Williams, J.J.; Ye, Y.Y.; Kramer, M.J.; Ho, K.M.; Hong, L.; Fu, C.L.; Malik, S.K. Theoretical calculations and experimental measurements of the structure of Ti_5Si_3 with interstitial additions. *Intermetallics* **2000**, *8*, 937–943. [CrossRef]
16. Du, W.; Zhang, L.; Ye, F.; Ni, X.; Lin, J. Intrinsic embrittlement of $MoSi_2$ and alloying effect on ductility: Studied by first-principles. *Phys. B Condens. Matter* **2010**, *7*, 1695–1700. [CrossRef]
17. Perdew, J.P.; Chevary, J.A.; Vosko, S.H.; Jackson, K.A.; Pederson, M.R.; Singh, D.J.; Fiolhais, C. Atoms, molecules, solids, and surfaces: Applications of the generalized gradient approximation for exchange and correlation. *Phys. Rev. B* **1992**, *11*. [CrossRef]
18. Vanderbilt, D. Soft self-consistent pseudopotentials in a generalized eigenvalue formalism. *Phys. Rev. B* **1990**, *11*. [CrossRef]
19. Pack, J.D.; Monkhorst, H.J. Special points for Brillouin-zone integrations—A reply. *Phys. Rev. B* **1977**, *4*. [CrossRef]
20. Chu, F.; Thoma, D.J.; McClellan, K.J.; Peralta, P. Mo_5Si_3 single crystals: Physical properties and mechanical behavior. *Mater. Sci. Eng. A* **1999**, *261*, 44–52. [CrossRef]
21. Kocherzhinskij, Y.A.; Kulik, O.G.; Shishkin, E.A. Phase diagram of the tantalum-silicon system. *Dokl. Akad. Nauk SSSR* **1981**, *261*, 106–108.

22. Fu, C.L.; Wang, X.; Ye, Y.Y.; Ho, K.M. Phase stability, bonding mechanism, and elastic constants of Mo_5Si_3 by first-principles calculation. *Intermetallics* **1999**, *2*, 179–184. [CrossRef]
23. Voigt, W. A Determination of the elastic constants for beta-quartz lehrbuch de kristallphysik. *Terubner Leipzig*. **1928**, *40*, 2856–2860.
24. Reuss, A. Berechnung der Fließgrenze von Mischkristallen auf Grund der Plastizitätsbedingung für Einkristalle. *ZAMM J. Appl. Math. Mech.* **1929**, *9*, 49–58. [CrossRef]
25. Hill, R. The elastic behaviour of a crystalline aggregate. *Proc. Phys. Soc. A* **1952**, *65*, 349–354. [CrossRef]
26. Brauer, G.; Zapp, K.H. Die nitride des tantals. *Anorg. Allg. Chem.* **1954**, *277*, 129–139. [CrossRef]
27. Wang, F.E.; Buehler, W.J.; Pickart, S.J. Crystal structure and a unique "Martensitic" transition of TiNi. *J. Appl. Phys.* **1965**, *36*, 3232–3239. [CrossRef]
28. Nowotny, H.; Laube, E. The thermal expansion of high-melting phases. *Plansee. Pulver.* **1961**, *9*, 85–92.
29. Jette, E.R.; Foote, F. Precision determination of lattice constants. *J. Chem. Phys.* **1935**, *3*, 605–616. [CrossRef]
30. Sakakibara, N.; Takahashi, Y.; Okumura, K.; Hattori, K.H.; Yaita, T.; Suzuki, K.; Shimizu, H. Speciation of osmium in an iron meteorite and a platinum ore specimen based on X-ray absorption fine-structure spectroscopy. *Geochem. J.* **2005**, *39*, 383–389. [CrossRef]
31. Zhang, C.; Han, P.; Li, J.; Chi, M.; Yan, L.; Liu, Y.; Liu, X.; Xu, B. First-principles study of the mechanical properties of NiAl microalloyed by M (Y, Zr, Nb, Mo, Tc, Ru, Rh, Pd, Ag, Cd). *J. Phys. D Appl. Phys.* **2008**, *41*. [CrossRef]
32. Featherston, F.H.; Neighbours, J.R. Elastic constants of tantalum, tungsten, and molybdenum. *Phys. Rev.* **1963**, *130*. [CrossRef]
33. McSkimin, H.J.; Andreatch, P., Jr. Elastic moduli of silicon *vs.* hydrostatic pressure at 25.0 °C and −195.8 °C. *J. Appl. Phys.* **1964**, *35*, 2161–2165. [CrossRef]
34. Kang, L.U.O.; Bing, Z.; Shang, F.U.; Jiang, Y.; Yi, D.Q. Stress/strain aging mechanisms in Al alloys from first principles. *Trans. Nonferr. Met. Soc. China* **2014**, *24*, 2130–2137.
35. Chu, F.; Lei, M.; Maloy, S.A.; Petrovic, J.J.; Mitchell, T.E. Elastic properties of C40 transition metal disilicides. *Acta Mater.* **1996**, *44*, 3035–3048. [CrossRef]
36. Tao, X.; Chen, H.; Tong, X.; Ouyang, Y.; Jund, P.; Tedenac, J.C. Structural, electronic and elastic properties of V_5Si_3 phases from first-principles calculations. *Comput. Mater. Sci.* **2012**, *53*, 169–174. [CrossRef]
37. Ström, E.; Eriksson, S.; Rundlöf, H.; Zhang, J. Effect of site occupation on thermal and mechanical properties of ternary alloyed Mo_5Si_3. *Acta Mater.* **2005**, *53*, 357–365. [CrossRef]
38. Pan, Y.; Lin, Y.; Xue, Q.; Ren, C.; Wang, H. Relationship between Si concentration and mechanical properties of Nb–Si compounds: A first-principles study. *Mater. Des.* **2016**, *89*, 676–683.
39. Pugh, S.F. XCII. Relations between the elastic moduli and the plastic properties of polycrystalline pure metals. *Lond. Edinb. Dublin Philos. Mag. J. Sci.* **1954**, *45*, 823–843. [CrossRef]
40. Chumakov, A.I.; Monaco, G.; Fontana, A.; Bosak, A.; Hermann, R.P.; Bessas, D.; Wehinger, B.; Crichton, W.A.; Krisch, M.; Baldi, G.; *et al.* Role of disorder in the thermodynamics and atomic dynamics of glasses. *Phys. Rev. Lett.* **2014**, *112*. [CrossRef] [PubMed]
41. Pettifor, D.G. Theoretical predictions of structure and related properties of intermetallics. *Mater. Sci. Technol.* **1992**, *8*, 345–349. [CrossRef]
42. Mukhanov, V.A.; Kurakevych, O.O.; Solozhenko, V.L. Thermodynamic aspects of materials' hardness: Prediction of novel superhard high-pressure phases. *High Press. Res.* **2008**, *28*, 531–537. [CrossRef]
43. Gilman, J.J. Hardness—A strength microprobe. In *The Science of Hardness Testing and Its Research Applications*; Westbrook, J.H., Conrad, H., Eds.; American Society of Metal: Metal Park, OH, USA, 1973.
44. Liu, A.Y.; Cohen, M.L. Structural properties and electronic structure of low-compressibility materials: β-Si_3N_4 and hypothetical β-C_3N_4. *Phys. Rev. B* **1990**, *41*, 10727–10734. [CrossRef]
45. Teter, D.M.; Bull, M.R.S. Hardness and fracture toughness of brittle materials. *Phys. Rev. B* **1998**, *23*. [CrossRef]
46. Chen, X.Q.; Niu, H.; Franchini, C.; Li, D.; Li, Y. Hardness of T-carbon: Density functional theory calculations. *Phys. Rev. B* **2011**, *84*. [CrossRef]
47. Tao, X.; Jund, P.; Colinet, C.; Tédenac, J.C. First-principles study of the structural, electronic and elastic properties of W_5Si_3. *Intermetallics* **2010**, *18*, 688–693. [CrossRef]
48. Mulliken, R.S. Electronic population analysis on LCAO–MO molecular wave functions. I. *J. Chem. Phys.* **1955**, *23*, 1833–1840. [CrossRef]

49. Cao, Y.; Zhu, P.; Zhu, J.; Liu, Y. First-principles study of NiAl alloyed with Co. *Comput. Mater. Sci.* **2016**, *111*, 34–40. [CrossRef]
50. Wang, H.Z.; Zhan, Y.Z.; Pang, M.J. The structure, elastic, electronic properties and Debye temperature of M2AlC (M = V, Nb and Ta) under pressure from first principles. *Comput. Mater. Sci.* **2012**, *54*, 16–22. [CrossRef]
51. Shi, S.; Zhu, L.; Jia, L.; Zhang, H.; Sun, Z. *Ab-initio* study of alloying effects on structure stability and mechanical properties of α-Nb_5Si_3. *Comput. Mater. Sci.* **2015**, *108*, 121–127. [CrossRef]
52. Chen, Q.; Sundman, B. Calculation of Debye temperature for crystalline structures—A case study on Ti, Zr, and Hf. *Acta Mater.* **2001**, *49*, 947–961. [CrossRef]
53. Du, L.; Wang, L.; Zheng, B.; Du, H. Numerical simulation of phase separation in Fe–Cr–Mo ternary alloys. *J. Alloy. Compd.* **2016**, *663*, 243–248. [CrossRef]
54. Cuenya, B.R.; Frenkel, A.I.; Mostafa, S.; Behafarid, F.; Croy, J.R.; Ono, L.K.; Wang, Q. Anomalous lattice dynamics and thermal properties of supported size-and shape-selected Pt nanoparticles. *Phys. Rev. B* **2010**, *82*. [CrossRef]